

UKAEA-CCFE-PR(19)69

Ruben Otin and Robert Salmon

# **A simplified methodology for the numerical assessment of welding workers exposure to electromagnetic fields**

Enquiries about copyright and reproduction should in the first instance be addressed to the  
UKAEA  
Publications Officer, Culham Science Centre, Building K1/0/83 Abingdon, Oxfordshire,  
OX14 3DB, UK. The United Kingdom Atomic Energy Authority is the copyright holder.

# **A simplified methodology for the numerical assessment of welding workers exposure to electromagnetic fields**

Ruben Otin and Robert Salmon



# A simplified methodology for the numerical assessment of welding workers exposure to electromagnetic fields

Ruben Otin<sup>1</sup> and Robert Salmon<sup>1</sup>

<sup>1</sup> *United Kingdom Atomic Energy Authority (UKAEA) - Culham Centre for Fusion Energy (CCFE)  
Culham Science Centre, OX14 3DB, Oxfordshire, United Kingdom*

*Correspondence to: Ruben Otin, United Kingdom Atomic Energy Authority, Culham Centre for Fusion Energy, J20/1/69, Culham Science Centre, OX14 3DB, Oxfordshire, United Kingdom. E-mail: ruben.otin@ukaea.uk*

## Abstract

The equipment used in some welding techniques (e.g. tungsten inert gas alternating current welding or capacitor discharge stud welding) can induce high electromagnetic fields inside the operator due to the large time-varying electric currents involved in the process. The European Union (EU) Directive 2013/35/EU provides guidelines and recommendations to guarantee the security and health of the operator by means of two sets of limit values: Action Levels (ALs) and Exposure Limit Values (ELVs). These limits are based on recommendations from the International Commission on Non-Ionizing Radiation Protection (ICNIRP) and are found in the Control of Electromagnetic Fields at Work (CEMFAW) 2016 Regulations.

In this paper we present a simplified methodology to calculate the ALs and ELVs. This methodology can be applied to any welding process that uses a time-varying electric current. The ALs and ELVs are obtained with the help of an in-house Python code and the open-source finite element software ERMES. The Python code applies the Weighted Peak Method (WPM) in frequency domain to measured current profiles and generates normalization constants that are used by ERMES to calculate the three-dimensional spatial distribution of ALs and ELVs. Finally, the three-dimensional maps obtained are used to assess the welding technique against the EU Directive 2013/35/EU.

**Keywords:** Directive 2013/35/EU; work safety; arc welding; resistance welding; weighted peak method; finite element method;

## 1. Introduction

Arc and resistance welding equipment can induce high electromagnetic fields (EMFs) inside the operator due to the large time-varying electric currents involved in the process and the proximity of the operator to the EMFs source. The European Union (EU) Directive 2013/35/EU (the Directive) [1] provides guidelines and recommendations to guarantee the security and health of the operator by means of two sets of limit values: Action Levels (ALs) and Exposure Limit Values (ELVs). These limits are applicable to workers not at particular risk and are based on the recommendations from the International Commission on Non-Ionizing Radiation Protection (ICNIRP). These limits are also found in the Control of Electromagnetic Fields at Work (CEMFAW) 2016 Regulations.

ELVs are the legal limits for exposure to EMFs, specified to protect workers from health and sensory effects. As they specify electric field levels of exposure within the body, they are often impossible or difficult to measure directly; they can only be obtained through computer modelling. These numerical simulations can be challenging due to the complex interaction of the induced electric field with the tissues of the human body. Therefore, to make things easier, there is a separate set of values, the ALs, which allow the assessment of the EMF exposure without considering the body of the operator. If the AL is exceeded, further consideration and assessment is required to determine whether the corresponding ELV may be exceeded. But if exposure is below the ALs, it will therefore be below the ELVs.

In this work we present a numerical approach to determine the ALs and ELVs of any welding process that uses time-varying electric currents as, for instance, the Tungsten Inert Gas-Alternating Current (TIG-AC) technique or the Capacitor Discharge (CD) stud welding.

The ALs and ELVs are obtained from measured current profiles with the help of an in-house Python code and the open-source finite element software ERMES [2]. The Python code applies the Weighted Peak Method (WPM) in frequency domain [1] to the measured current profile and generates normalisation constants that are used by ERMES to calculate the three-dimensional spatial distribution of ALs and ELVs. Finally, the three-dimensional maps obtained are used to assess the welding technique against the EU Directive 2013/35/EU.

This article is organized as follows: Sections 2.1 and 2.2 explain in more detail the meaning of ALs and ELVs. These sections are a summary of the definitions and explanations given in reference [1] and are presented here just for making the paper self-content. Sections 2.3 and 2.4 describe the methods and procedures used to compute the ALs and ELVs. Sections 3 and 4 apply the methodology unfolded in the previous sections to the TIG-AC and CD stud welding techniques as examples of application. At the end of sections 3 and 4 the corresponding welding process is assessed against the EU Directive and actions to guarantee compliance proposed. These actions and further conclusions are summarized in section 5.

## **2. Calculation of electromagnetic exposure levels**

As explained in the introduction, ALs and ELVs are two sets of limit values applicable to workers not at particular risk for the assessment of EMF exposure. Workers not at particular risk are those not having active implants, prosthesis, being pregnant, or another specific situation which will require a further, more personalized, risk assessment. The risk assessment guidelines for workers at particular risk are specified in the Council Recommendation 1999/519/EC and are not treated here. In this work we focus our attention on the calculation of the electromagnetic exposure limit levels for non-thermal direct effects in the frequency range of interest in welding (from 0 Hz to 10 MHz).

Direct effects are those arising from an interaction of the fields with the body and may be either non-thermal or thermal in nature. In the frequency range of interest for welding applications we are mainly dealing with non-thermal effects. Non-thermal, direct effects at low frequency include: vertigo and nausea from static magnetic fields and effects on sense organs, nerves and muscles. Indirect effects such as interference with electronic equipment, interference with active or passive implanted medical devices, effects on shrapnel, body piercings, projectile risk from loose ferromagnetic objects, unintentional initiation of detonators, fires or explosions, electric shocks or burns from contact currents, etc, are not treated here and must be the subject of another risk assessment dedicated to analysing the work environment.

### **2.1. Action Levels (ALs)**

ALs correspond to calculated or measured electric and magnetic field values at the workplace in the absence of the worker. ALs allow for a simple conservative exposure assessment which guarantees the automatic compliance with ELVs. If the operator works in an area in which the ALs are below the calculated or measured limits then, it is guaranteed that the electric and magnetic fields inside the operator's body are below the ELVs and further assessment is not needed [1].

For the electric field exposure, two sets of values are considered (Directive 2013/35/EU, Annex II):

- Low ALs are based on limiting the internal electric field below the ELVs and limiting spark discharges in the working environment.
- High ALs guarantee that the internal electric field does not exceed the ELVs and spark discharges are prevented, provided that the protection measures referred to in the Article 5(6)

of the Directive are taken. Article 5(6) refers to protection measures such as grounding of work objects, bonding of workers with work objects and the use of protective equipment. Then, the difference between high and low electric field exposure ALs is that in the high AL is assumed that the protective measures specified in Article 5(6) are present in the workplace.

For the magnetic field exposure, three sets of values are considered (Directive 2013/35/EU, Annex II):

- Low ALs are, for frequencies below 400 Hz, derived from the sensory effects ELVs (to be discussed in the next section) and, for frequencies above 400 Hz, from the health effects ELVs for internal electric field.
- High ALs are derived from the health effects ELVs for internal electric field related to electric stimulation of peripheral and autonomous nerve tissues in head and trunk. Compliance with the high ALs ensures that health effects ELVs are not exceeded, but the effects related to retinal phosphenes and minor transient changes in brain activity are possible, if the exposure of the head exceeds the low ALs for exposures up to 400 Hz. In such a case, Article 5(6) applies.
- Limbs ALs are derived from the health effects ELVs for internal electric field related to electric stimulation of the tissues in limbs by taking into account that the magnetic field is coupled more weakly to the limbs than to the whole body.

There are also ALs for static magnetic fields and contact currents. The static magnetic flux density ALs applies to workers at particular risks and to indirect effects. In this report we focus our attention on non-thermal, direct effects for workers not at particular risk. Therefore, static ALs are not treated here. We also assume that the worker is not in direct contact with the cable that carries the electric current and, therefore, we do not consider the contact current ALs in this report.

Tables with all the ALs limit values detailed above and further details are given in Annex II of the EU Directive 2013/35/EU, which can be found in the reference [1, Appendix L]. To calculate the ALs for a multiple frequency exposure we used the Weighted Peak Method (WPM) of section 2.3 combined with the Finite Element Method (FEM) model explained in sections 2.4.

## **2.2. Exposure Limits Values (ELVs)**

ELVs are values established based on biophysical and biological considerations, in particular based on scientifically well-established short-term and acute direct effects such as thermal effects and electrical stimulation of tissues [1].

Two sets of values are considered (Directive 2013/35/EU, Annex II):

- Health effects ELVs' means those ELVs above which workers might be subject to adverse health effects, such as thermal heating or stimulation of nerve and muscle tissue. Health effects ELVs are related to electric stimulation of all peripheral and central nervous system tissues in the body, including the head. Health effects ELV for controlled working conditions is applicable on a temporary basis during the shift when justified by the practice or process, provided that preventive measures, such as controlling movements and providing information to workers, have been adopted.
- Sensory effects ELVs' means those ELVs above which workers might be subject to transient disturbed sensory perceptions and minor changes in brain functions. The sensory effects ELVs are related to electric field effects on the central nervous system in the head, i.e. retinal phosphenes and minor transient changes in some brain functions. The sensory effects ELV is the ELV for normal working conditions and is related to vertigo and other physiological effects related to disturbance of the human balance organ resulting mainly from moving in a static magnetic field

There are also ELVs for the external magnetic flux density at frequencies going from 0 to 1 Hz. But, for welding applications, the static fields are usually far below the limits specified for workers not at particular risk in normal working conditions.

Tables with all the ELVs detailed above and further details are given in Annex II of the EU Directive 2013/35/EU, which can be found in the reference [1, Appendix L]. To calculate the ELVs for multiple frequency exposure we used the WPM and the FEM model explained in the following sections.

### 2.3. Weighted Peak Method (WPM) in frequency domain

The WPM in frequency domain is the method recommended in [1] to calculate compliance with either the ALs or ELVs from multiple frequency exposure. The steps required to perform the WPM are shown in Figure 1 and explained in the following. First, the amplitudes of the spectral components that make up the electrical current signal are divided by the frequency-dependent ALs/ELVs coefficients provided in the Annex II of the Directive 2013/35/EU. Secondly, a phase is added to the phase of each spectral component as show in Equation 1. The value of the added phase changes depending on how the corresponding AL/ELV weight varies with frequency (see Equation 1). Then, the weighted spectrum is converted back to the time domain using Equation 1. Finally, the exposure index is obtained from the peak of the time-domain waveform. The exposure index is complaint with the directive if it is lower than 1 (or to 100% if given as a percentage) and non-complaint if it is greater than 1 (or 100%). The same formula given in Equation 1 is used to calculate ELVs by just replacing AL with ELV and removing the constant  $\sqrt{2}$  (ELVs are defined as peak values in the Directive, unlike the ALs, which are defined as Root-Mean-Square).

The WPM method was implemented in an in-house Python code. This code reads a file containing measured electrical currents as a function of time and generates the input data required by ERMES to visualize the three-dimensional exposure limit maps. How ERMES generates these results is the objective of the next section.

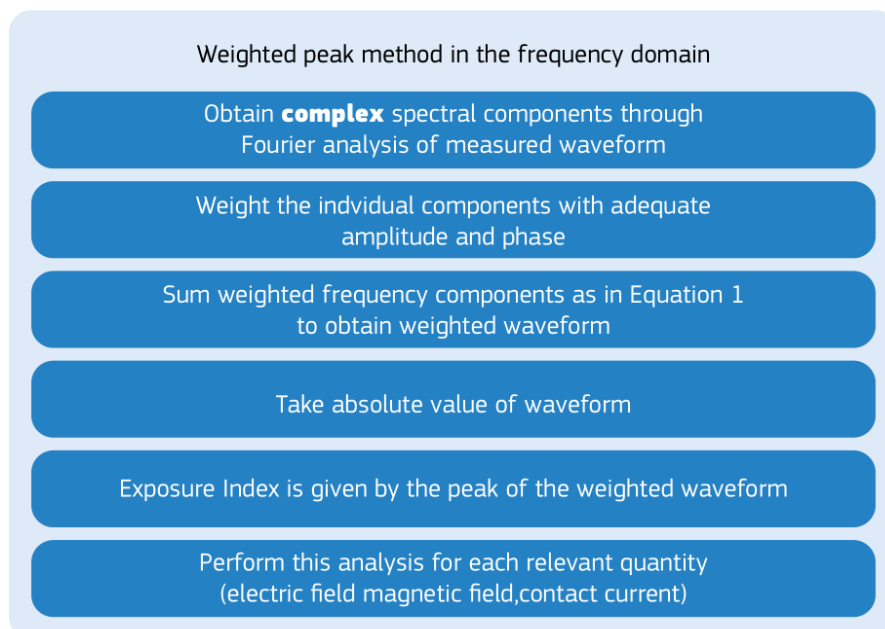


Fig. 1. Outline of the Weighted Peak Method (WPM) in frequency domain as given in [1].

$$EL_{non-thermal}^{WP} = \text{Maximum} \left\{ \left| \sum_f \frac{|A_f|}{AL_f \sqrt{2}} * \cos(2\pi f t + \theta_f + \varphi_f) \right| \right\}$$

$$\varphi_f = \begin{cases} 180^\circ, f \text{ or } AL_f \propto 1/f^2 \\ 90^\circ, f \text{ or } AL_f \propto 1/f \\ 0^\circ, f \text{ or } AL_f = \text{constant} (\propto f^0) \\ -90^\circ, f \text{ or } AL_f \propto f \end{cases}$$

Equation 1. Expression used in the WPM to convert the weighted spectrum of a signal to the time domain and extract the exposure index (from [1]).  $EL^{WP}$  stands for Exposure Limit (AL or ELV) calculated by the Weighted Peak (WP) method,  $|A_f|$  and  $\theta_f$  are the peak amplitude (electric field strength or magnetic flux density) and phase of the spectral component at frequency  $f$  respectively.  $AL_f$  is the relevant AL at that frequency. The phase  $\varphi_f$  is a function of frequency and is defined in the appendix of the ICNIRP 2010 guidelines. The same expression can be used to calculate the ELVs by just replacing AL with ELV and removing the constant  $\sqrt{2}$  (ELVs are defined as peak values).

## 2.4. ERMES finite element model

The electromagnetic fields generated in the welding process and their interaction with the operator are calculated using the open-source software ERMES [2]. ERMES implements in C++ a frequency domain FEM formulation which is a simplified version of the weighted regularized Maxwell equation method [3]. This FEM formulation produces well-conditioned matrices which can be solved efficiently with low-memory consuming iterative methods. Also, thanks to the null kernel of its differential operator, it can operate indistinctly in high and low frequency regimes. ERMES is a versatile tool which had been applied to a wide variety of scenarios such as microwave engineering [3], specific absorption rate computations [3, 4, 6, 7], electromagnetic compatibility [5, 10] and electromagnetic forming [8, 9]. Validations of ERMES against measurements, analytical methods and other numerical software can be found through all the above-mentioned references [2-10].

One of the main advantages of ERMES for the application discussed in this report is that it can solve the full set of time-harmonic Maxwell equations at any frequency. This makes possible to consider inductive and capacitive effects simultaneously at low frequencies. This feature it is not easily found in commercial codes and it usually requires specialized software as, for instance, the ones shown in references [11, 12]. The importance of this feature in the electromagnetic exposure assessment against the Directive is explained in the following paragraph.

In time-harmonic electromagnetic problems the currents induced inside a body have two main contributions: the eddy currents ( $\mathbf{J}_e = \sigma \mathbf{E}$ ) and the displacement currents ( $\mathbf{J}_d = i\epsilon\omega \mathbf{E}$ ), where  $\epsilon$  is the electrical permittivity,  $\sigma$  the electrical conductivity,  $\omega$  the angular frequency and  $i$  the imaginary unit. At low frequencies we usually have that  $\sigma \gg \epsilon\omega$  and the eddy currents dominate. But, due to the high electrical permittivity of the human tissue at low frequencies, we can find that the assumption  $\sigma \gg \epsilon\omega$  is no longer valid in some cases and the displacement currents must be considered.

Table 1 and 2 show a few values of  $\epsilon\omega$  and  $\sigma$  taken from [13] at the frequencies that correspond with the frequencies of the main harmonic in the CD stud welding technique (40 Hz) and the TIG-AC process (120 Hz) analysed in the next sections. As can be observed in the Table 1 and 2,  $\epsilon\omega$  can be of similar order or even greater than  $\sigma$  and this effect is more accentuated in the CD stud case.

### 2.4.1. FEM model

The geometry used by ERMES to calculate the electromagnetic fields is shown in Fig. 2. This configuration was selected after the ones proposed in [14] for CD stud and TIG-AC welding. We modified the basic geometries of [14] to consider general good practices followed by our operators (no cable over shoulder, stay outside the current loop) and worst-case scenario disposition between cable and operator (cable parallel to the leg implies that the electric field is parallel to the mannequin surface and is not attenuated by induced electric charges).

The source of the fields is a time-harmonic electric current density  $\mathbf{J}$  oscillating at the frequency  $\omega$  and following the cable path shown in Figure 2. The cabling to the power supply was neglected considering that, after some distance from the working area the cables are paired, and that they do not generate any appreciable field. The dimensions of the cable loop were obtained from standard scenarios of the welding set-ups used on-site. The fields generated by the power supply were also neglected considering its distance to the working area.

A workbench table was placed close to the welder operator just to serve as a geometrical reference. No electrical properties were assigned to this table. The operator mannequin was assumed electrically homogeneous. As it is explained later, it is acceptable to assess compliance to the Directive by applying extreme values of electrical permittivity and conductivity to a homogeneous mannequin, as opposed to assigning organ specific values.

The electromagnetic FEM model was enclosed by a spherical surface with a diameter of 8 m centered in the welder operator (see Figure 3). On this surface was assumed that the tangential component of the magnetic field was zero. This boundary condition is an excellent approximation in our model due to the fact that the fields are strongly localized around the current loop and that they attenuate very fast with the distance.

The geometry was meshed using second order isoparametric tetrahedral finite elements. Different element sizes were used to check convergence and virtually no variation of the results were observed from meshes varying from  $1e6$  to  $3e6$  elements. A few pictures of the FEM mesh are shown in Figure 4.

The sparse linear system emerging from the FEM discretization was solved using a diagonally preconditioned Transpose-Free Quasi-Minimal Residual (TFQMR) iterative solver with a residual error of  $1e-9$ . The number of complex unknowns varied from  $6e6$  to  $11e6$ . The time required to solve the linear system in a 64-bit Windows 7 Professional OS, Intel(R) Core(TM) i7-4790K CPU @ 4.00GHz, 32 GB of RAM varied from 40 minutes to a few hours depending of the mesh used.

Table 1. Electrical properties of some human tissues at  $f = 40$  Hz from [13]. Being  $\epsilon_r$  the relative electrical permittivity,  $\sigma$  the electrical conductivity in S/m,  $\omega (=2\pi f)$  the angular frequency in Hz and  $\epsilon\omega = \epsilon_r\epsilon_0\omega$  with  $\epsilon_0 = 8.854e-12$  F/m the permittivity of vacuum.

	$\epsilon_r$	$\epsilon\omega$	$\sigma$
Brain	1.64e7	0.04	0.09
Heart	1.13e7	0.02	0.08
Kidney	1.33e7	0.03	0.08
Lung	8.24e6	0.02	0.06
Muscle	2.00e7	0.04	0.22
Intestine	3.46e7	0.08	0.04

Table 2. Electrical properties of some human tissues at  $f = 120 \text{ Hz}$  from [13]. Being  $\epsilon_r$  the relative electrical permittivity,  $\sigma$  the electrical conductivity in S/m,  $\omega (=2\pi f)$  the angular frequency in Hz and  $\epsilon\omega = \epsilon_r\epsilon_0\omega$  with  $\epsilon_0 = 8.854\text{e-}12 \text{ F/m}$  the permittivity of vacuum.

	$\epsilon_r$	$\epsilon\omega$	$\sigma$
Brain	2.84e6	0.02	0.11
Heart	2.39e6	0.02	0.09
Kidney	2.59e6	0.02	0.10
Lung	1.31e6	0.01	0.07
Muscle	7.43e6	0.05	0.27
Intestine	1.65e7	0.11	0.14

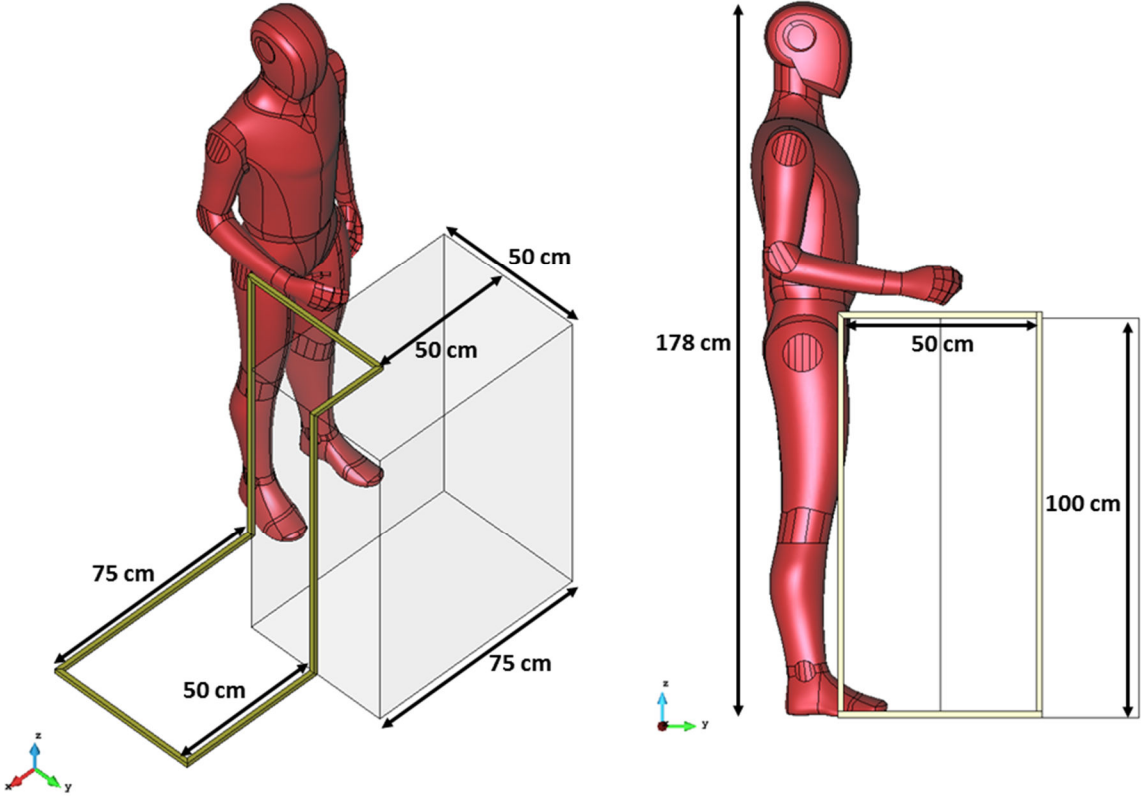


Fig. 2. CAD geometry and dimensions of the operator's mannequin, cable and workbench table.

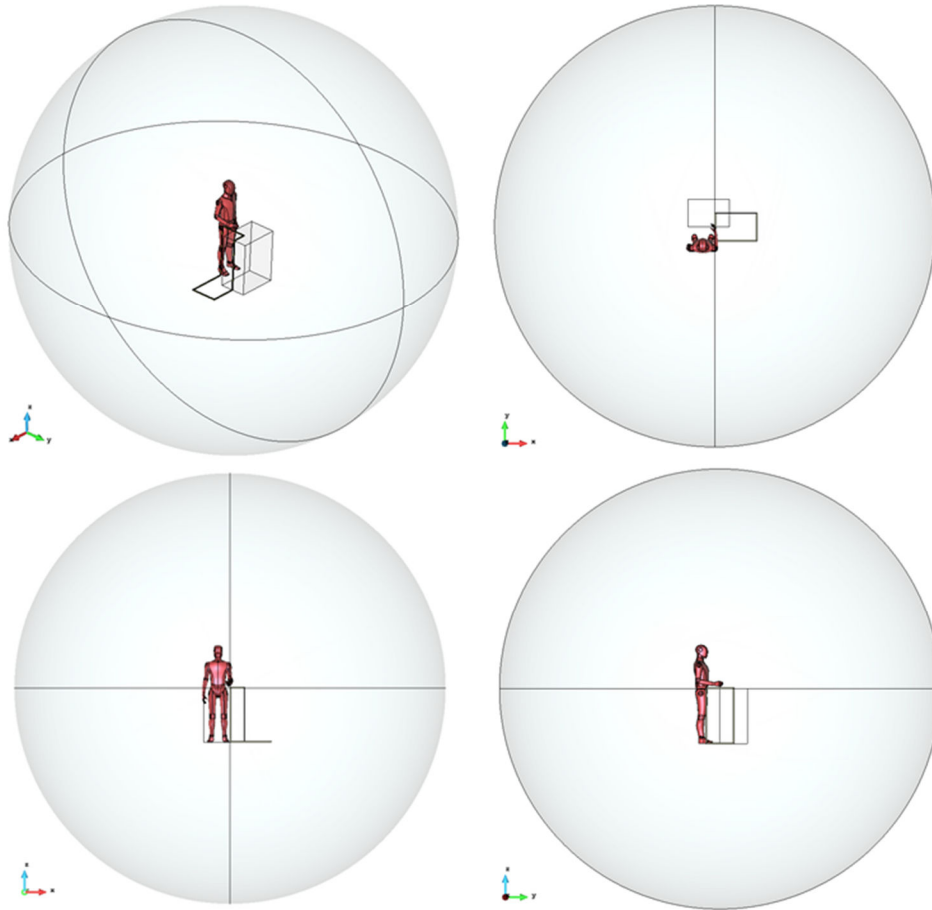


Fig. 3. Electromagnetic FEM model. The operator's mannequin, cable and workbench table is located at the centre of an 8 m diameter sphere. A far field boundary condition was applied to the exterior surface of the sphere. The volume of the sphere (including mannequin, cable and table) was meshed with second order isoparametric tetrahedral finite elements.

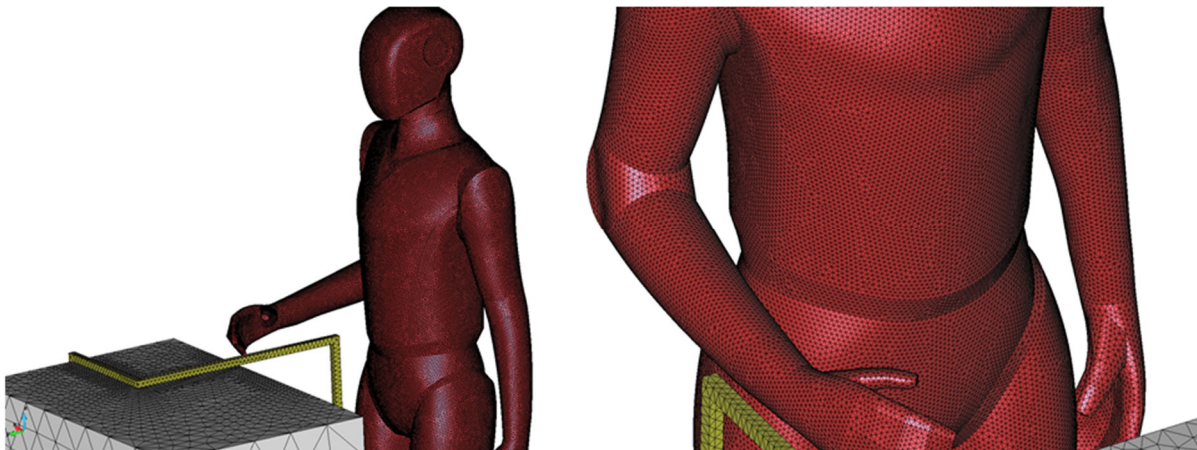


Fig. 4. Details of the FEM mesh. The geometry was meshed using between 1e6 and 3e6 second order isoparametric tetrahedral finite elements. Different mesh sizes were tested to check convergence.

#### 2.4.2. Computing ALs

The ALs are calculated following the steps given in Figure 1. The first step is to apply the Fourier transform to the current intensity profile of the welding process under consideration. Then, the electromagnetic fields generated by each spectral component are calculated using the FEM model discussed in the previous section. Finally, ALs are obtained by applying Equation 1 to the calculated

fields at every node of the FEM mesh. The FEM computations required in this process can be speeded up by applying the simplifications explained in the following.

The first simplification is that it is not necessary to assign electric properties to the mannequin (which is merely used as a geometric reference). This is so because the ALs correspond to calculated or measured electromagnetic field values in the absence of the welder operator.

The second simplification is that the fields generated by every spectral component of the current can be obtained from just one FEM simulation at 1 Hz and with a current intensity of 1 A flowing through the cable. This can be done thanks to the low-frequency nature of the problem and to the absence of materials in the problem domain. At low-frequencies, and without materials present, the magnetic flux density  $\mathbf{B}$  is independent of the frequency and proportional to the current. On the other hand, under the same conditions, the induced electric field  $\mathbf{E}$  depends linearly on frequency and current. Therefore, if  $\mathbf{B}_n$  and  $\mathbf{E}_n$  are the fields calculated in the 1 Hz – 1 A simulation then, the fields  $\mathbf{E}$  and  $\mathbf{B}$  generated by a spectral component of amplitude  $I_f$  and phase  $\varphi_f$  at the frequency  $f$  are:

$$\begin{aligned}\mathbf{B} &= \mathbf{B}_n \cdot I_f \cdot \exp(i\varphi_f), \\ \mathbf{E} &= \mathbf{E}_n \cdot I_f \cdot \exp(i\varphi_f) \cdot f.\end{aligned}$$

Now, we can substitute  $\mathbf{E}$  and  $\mathbf{B}$  in Equation 1 by the above relations. The fields  $\mathbf{B}_n$  and  $\mathbf{E}_n$  can be placed outside the summation over the frequency because they just depend on the position and are independent of the frequency. Therefore, the three-dimensional map representing an AL can be generated by multiplying the FEM calculated  $\mathbf{B}_n$  and  $\mathbf{E}_n$  by a global constant that is independent of the position and accounts for the spectrum of the current and the weights of the AL under consideration. These global constants are calculated with an in-house Python code and are used by ERMES to visualize the ALs.

In ERMES, the non-compliant region is enclosed by a surface surrounding the current source. This surface is the region of space in which the AL under study is equal to 1 (or 100% if given as a percentage). If the operator is outside this volume, then the welding process is compliant with the Directive and no more actions are required. On the other hand, if the operator is totally or partially inside the volume then the process is non-compliant with the ALs and further actions are required. These actions can consist, for instance, in computing the ELVs to show compliance with the Directive or moving the operator further away from the current to a compliant area.

### 2.4.3. Computing ELVs

The steps given in Figure 1 and the formula of Equation 1 can also be used to calculate ELVs by just replacing AL with ELV and removing the constant  $\sqrt{2}$  (ELVs are defined as peak values in the Directive unlike the ALs which are defined as Root-Mean-Square). The main difference with the previous case is that now we must consider the electric properties of the welder operator's body. Although this complicates a bit the assessment of the ELVs with respect to the ALs, we can make the computations of ELVs easier and faster by applying the simplifications explained in the following.

The main simplification we are going to apply consists in considering the operator's body electrically homogeneous. Although in [1] is recommended the use of heterogeneous realistic human models, as the ones provided in [13], we will show that this complication is unnecessary for the cases studied here. Our approach is similar to the one followed by the IEEE Standard 1528 [15] and the IEC 62209-1 protocol [16]. In these protocols a Specific Anthropomorphic Mannequin (SAM) phantom model with homogeneous frequency-dependent properties is used for the calculation of the Specific Absorption Rate (SAR).

In our case, we can apply the homogeneous body simplification because, in general, the exposure assessment against the Directive does not require the accurate electromagnetic energy deposition dosage that it is usually necessary in other applications as, for instance, hyperthermia treatments or Magnetic Resonance Imaging (MRI) modelling. For the application treated in this report, it is only required to

show that the field values are under (or above) the Directive limits in a worst-case scenario situation and, as we show later, this can be achieved with a homogeneous mannequin. But first, we are going to analyse how the electric field interacts with the mannequin.

From the Maxwell's equations we can obtain the relation between the components of the electric field at the surface separating two different media:

$$\begin{aligned}\mathbf{n} \cdot (\epsilon_1 \mathbf{E}_1) &= \mathbf{n} \cdot (\epsilon_2 \mathbf{E}_2), \\ \mathbf{n} \times \mathbf{E}_1 &= \mathbf{n} \times \mathbf{E}_2,\end{aligned}$$

where  $\epsilon (= \epsilon + i\sigma/\omega)$  is the complex permittivity of the media and  $\mathbf{n}$  the unit normal of the discontinuity surface pointing from region 2 into 1. The first equation states that the normal component of the electric field is discontinuous at the surface separating two different media and that the value of this discontinuity depends on the ratio of the complex permittivities of the two media. The second equation states that the tangential component has the same value at both sides of the material interface and, therefore, it is continuous at the surface separating two different media.

A consequence of the above relations is that, in general, the field inside the body with the higher complex permittivity will be smaller than the field outside. The higher the value of the permittivity is, the lower the value of the electric field inside the body will be. For a high enough permittivity, the normal component will be negligible with respect the tangential component and from that point on, almost no changes will be observed in the fields for further increases of the permittivity. This general behaviour can change slightly in some areas depending of geometrical features (re-entrant surfaces, corners or edges) and the relative direction of the external fields with respect to the body surface.

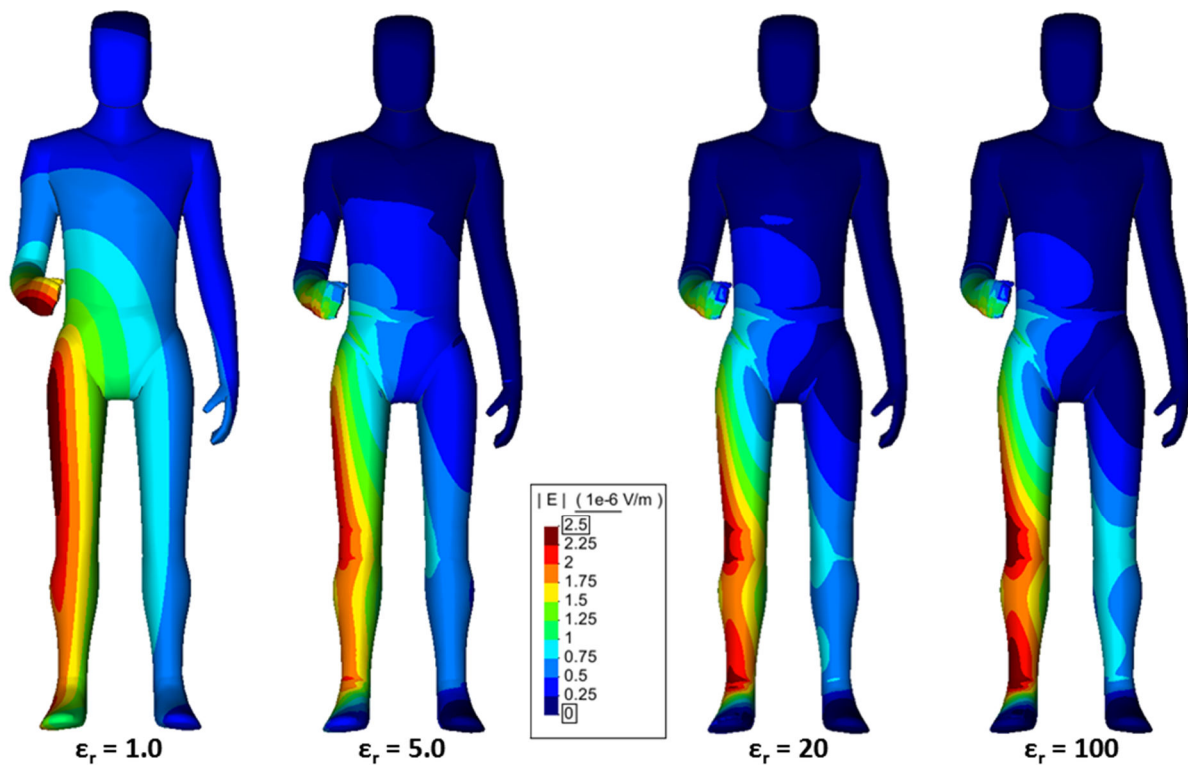


Fig. 5. Module of the electric field inside the homogeneous mannequin for different values of the electric permittivity. The fields are generated by an electric current of 1 A oscillating at 1 Hz. The electric conductivity is zero in all the cases. The same scale is used in all the figures for a better appreciation of the evolution of the electric field. See section 2.4.1 for a description of the FEM model.

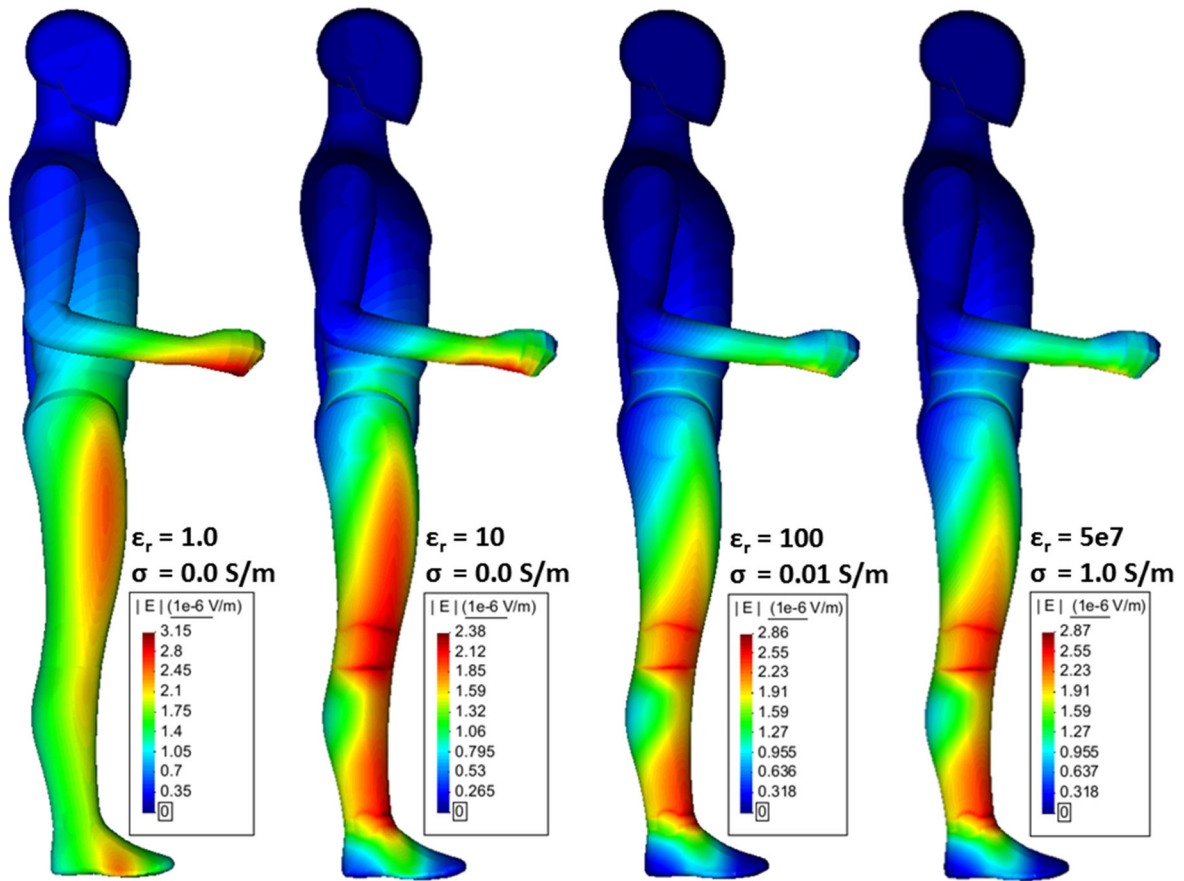


Fig. 6. Module of the electric field inside the homogeneous mannequin for different values of the electric permittivity and conductivity. The fields are generated by an electric current of 1 A oscillating at 1 Hz. The maximum electric field reached in each case is shown at the corresponding scale. See section 2.4.1 for a description of the FEM model.

Figure 5 and 6 show the evolution of the electric field for different values of  $\epsilon_r$  and  $\sigma$  for the geometry used in this study (see section 2.4.1 for a description of the FEM model). In Figure 5 we can see how the electric field  $\mathbf{E}$  is concentrated in some areas but is reduced in others. The volume average of  $\mathbf{E}$  reduces with increasing permittivity although the maximum field at some spots can increase. Nevertheless, these point-wise maximums at high permittivities are always smaller than the maximum fields obtained with  $\epsilon_r=1$  and  $\sigma=0$  (see Figure 6). In Figure 6 we can also observe the saturation effect described in the above paragraph: for  $\epsilon_r > 100$  the field distribution inside the body almost does not change.

From the above discussion we can conclude that the worst-case scenario (maximum internal electric fields) happens for  $\epsilon_r=1$ ,  $\sigma=0$  and that the best-case scenario (minimum volume average of the internal electric fields) can be calculated using any high enough value of the pair  $\epsilon_r$  and  $\sigma$ ; the higher the better. We also tested different multilayer configurations of dielectrics and the above observation for the minimum and maximum field remains. That is, no matter the combination of dielectric layers, the field inside the body is always smaller than when all layers have  $\epsilon_r=1$ ,  $\sigma=0$  and has always a larger volume average that when all layers have the highest  $\epsilon_r$ ,  $\sigma$ .

Therefore, to show compliance with the Directive we first start by calculating the fields for  $\epsilon_r=1$  and  $\sigma=0$ . If the ELVs derived from these fields are below the limits, then we can be sure that the welding process under study is compliant. However, if the limits are exceeded that does not mean automatically that the welding process is non-compliant, because this approach is very conservative. Before declaring the process non-compliant we must see first what the lower limits of the fields are. That is, we must calculate the ELVs applying a high permittivity to the mannequin. Depending on how far or close the

calculated ELVs are from the limits, we can assess if the process is compliant or non-compliant. In this assessment we must consider that the real value of the ELVs is somewhere between the two extreme limits obtained. On the other hand, if the ELVs using the minimum fields approach are above the limits, then we can be sure that the welding process under study is non-compliant.

The maximum values of the permittivity and conductivity in the frequency range of interest can be obtained from [13]. From there, we obtained  $\epsilon_r=5e7$  and  $\sigma=1$  S/m as the maximum values. These are the values used in the assessments of the best-cases (minimum volume average of the internal electric fields) in sections 3 and 4.

Thanks to the simplification of using just one complex permittivity for all the frequencies and due to the low frequency nature of the fields and the low conductivities involved, we can calculate  $\mathbf{E}$  for any frequency and current from the normalized field  $\mathbf{E}_n$  as it is done in section 2.4.2. That is, if  $\mathbf{E}_n$  is the field obtained for a current of 1 A at 1 Hz then the electric field  $\mathbf{E}$  generated by a current of amplitude  $I_f$  and phase  $\varphi_f$  at the frequency  $f$  is:

$$\mathbf{E} = \mathbf{E}_n \cdot I_f \cdot \exp(i\varphi_f) \cdot f.$$

Then, the ELVs can be calculated following the same procedure explained in section 2.4.2 for the ALs. The global constants required by ERMES to visualize the ELVs are also obtained using the in-house Python code mentioned previously.

### **3. Tungsten Inert Gas-Alternating current (TIG-AC) welding process**

TIG welding is an arc welding process that uses a tungsten electrode to generate an arc to the surface of the target metal. The point where the arc meets the target metal has a high resistance and so produces a lot of heat melting the local metal surface. A consumable filler rod is fed into the welding pool at the arc point to generate a weld. This process must be carefully controlled and is nearly always performed using a hand-held welding torch.

TIG welding can be operated using a DC or AC power supply though it must be current controlled. TIG-AC welding is required for aluminium welding due to the surface oxide film. It is usual for a TIG-AC power supply to allow the operator to choose the positive and negative amplitude and frequency of the current, allowing for fine tuning to specific materials.

For the cases analysed in this report a Kemppi MasterTIG 3500W was used and the current measurements were taken using a PEM 20 kA Rogowski coil. To increase accuracy and sensitivity the Rogowski coil was set to 10 kA and wrapped twice around the power cable to the welding torch. Two examples of waveform from the AC Kemppi MasterTIG 3500W welder as used by UKAEA are shown in the following section.

#### **3.1. Current profiles**

Figures 7 and 9 show two examples of the current profiles generated by the AC Kemppi MasterTIG 3500W welder for two different configurations of the machine. The pulses in each current waveform are not exactly equal and so the ALs or ELVs were calculated for each pulse, using the process in Figure 1, and then the average AL or ELV for the pulse train was calculated. Figures 8 and 10 show the Fourier transforms of one of the pulses that made up the corresponding waveform. It can be observed that the frequency of the main harmonic corresponds to the one specified in the machine settings. Eight different current profiles were studied and the results of the worst-case scenarios are shown in the following sections.

#### **3.2. Action Levels**

The ALs for the TIG-AC welding process were calculated following the steps explained in section 2.4.2. We computed the limbs, high and low ALs for eight different waveforms and compare these ALs between them. Figures 11 and 12 show the worst case for the limbs AL. Figures 13 and 14 show the

worst case for the high and low ALs. Low and high ALs are represented in the same figure because they are practically the same at this frequency range.

Some intersection of the mannequin with the high/low AL non-compliant volume can be observed in Figures 13 and 14. Then, an evaluation of the ELVs is required and the results of this evaluation are presented in Figures 15 and 16 of section 3.3.

In the TIG-AC process analysed here the induced electric field ALs can be neglected because of its low value even for the worst-case scenario (low AL for  $E$  is below 4% of the permitted limits and high AL for  $E$  is below 1% of the permitted limits).

The static electric fields can be neglected for this low-voltage high-current process with the power source far from the working area. The static magnetic flux density  $B$  is lower than 0.5 mT in all the working area.

### 3.3. Exposure Limit Values

As explained in the previous section the high/low ALs were slightly exceeded in the working area (see Figures 13 and 14). Therefore, it was necessary to calculate the ELVs. The results are shown in Figure 15 and 16. We can see that the ELVs are compliant with the Directive: the worst-case health effect ELV is 82% of the limit and the worst-case sensory effect ELV is 46.1% of the limit. For the best-case scenario we have that the health effect ELV is 74.6% of the limit and the sensory effect ELV is 41.9% of the limit.

The ELVs were calculated using the methodology explained in section 2.4.3 and, even after applying this conservative approach, the exposure values are below the limits.

### 3.4. Risk assessment

No further actions are required because the process is compliant with the Directive, though the operator should be aware of the cable configurations used in this study. It is important that the operator does not stand within the current loop and makes reasonable efforts to route the current carrying cable away from themselves.

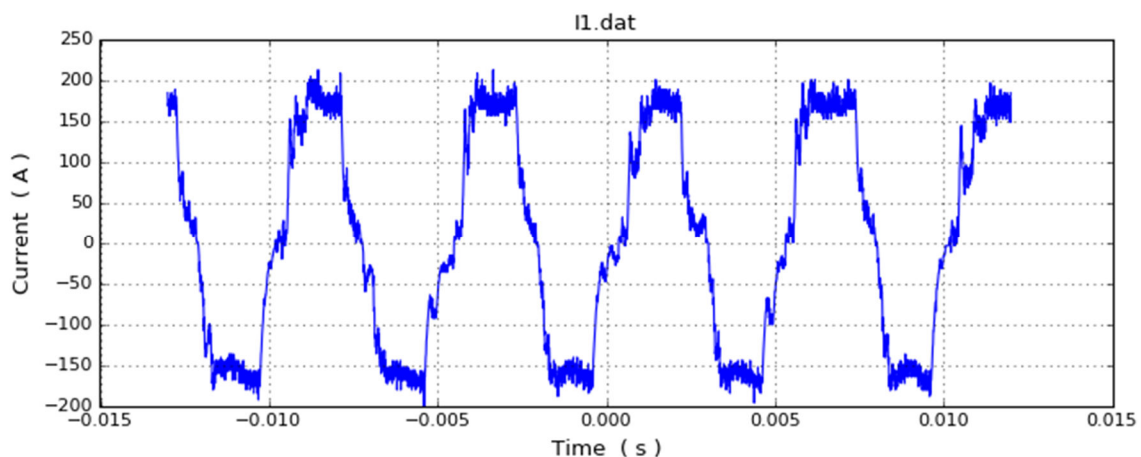


Fig. 7. TIG-AC current waveform for Kemppi MasterTIG 3500W machine settings: 140 A, 50% balance (50:50) and  $f = 200$  Hz.

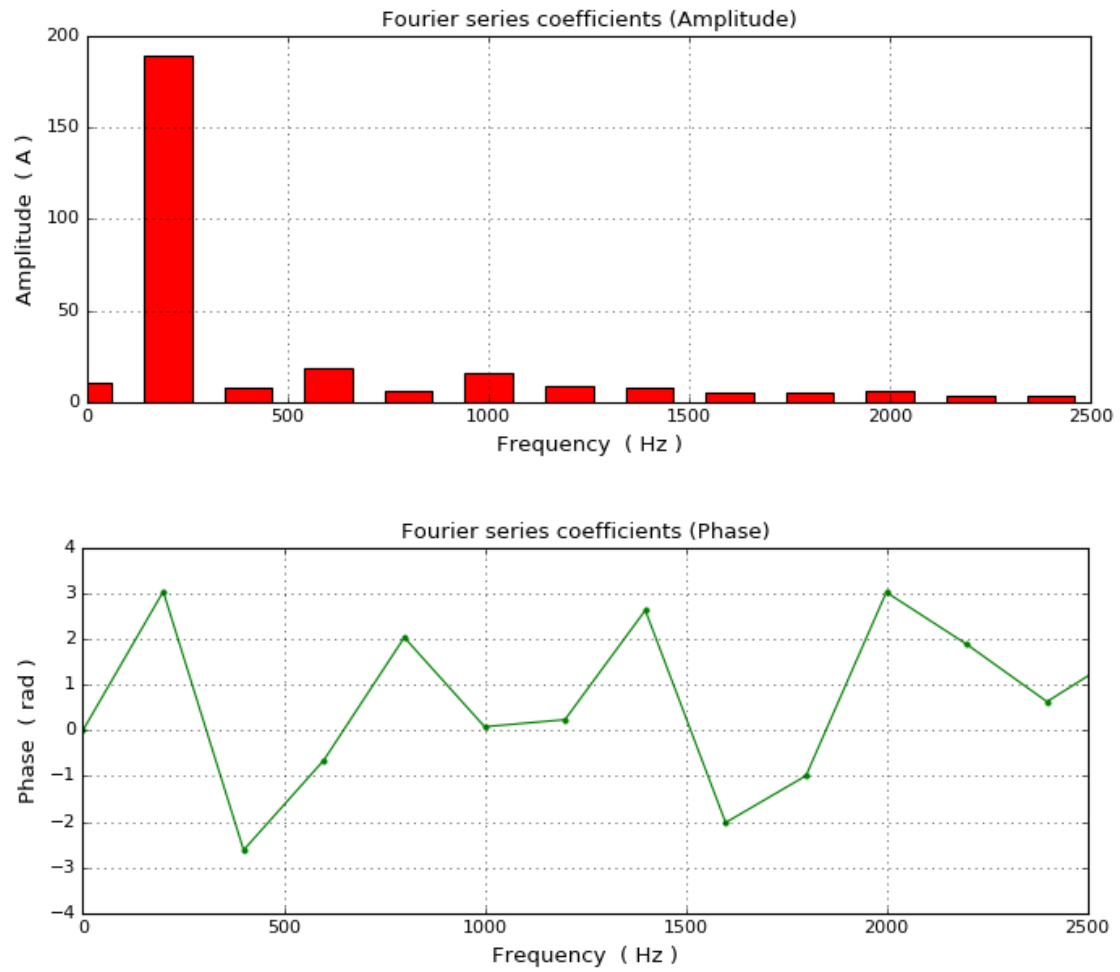


Fig. 8. Amplitude and phase of the first Fourier transform components of one of the pulses of the waveform shown in Figure 7.

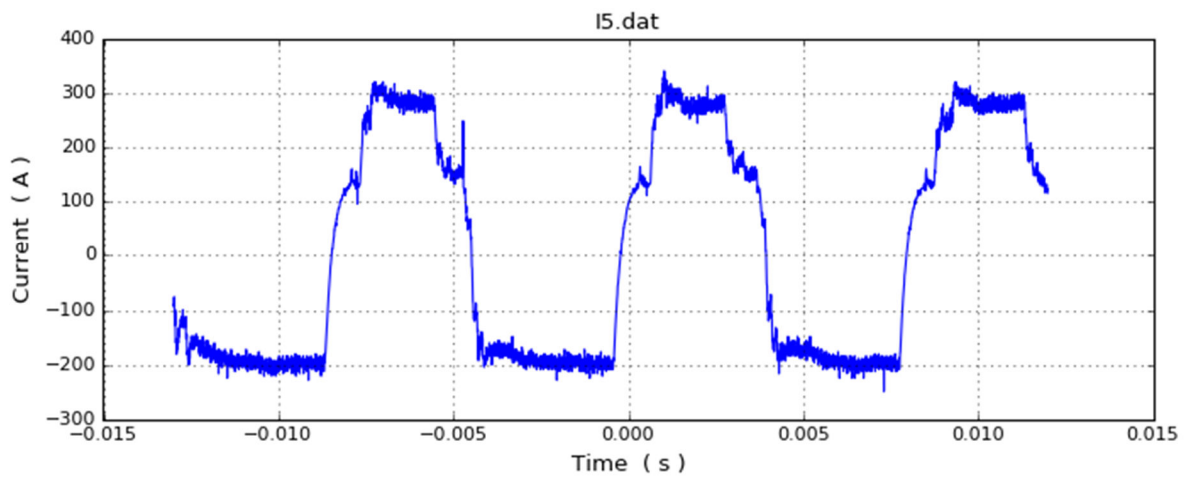


Fig. 9. TIG-AC waveform for Kemppi MasterTIG 3500W machine settings: 250 A, 65% negative balance (backwards) and  $f = 120$  Hz.

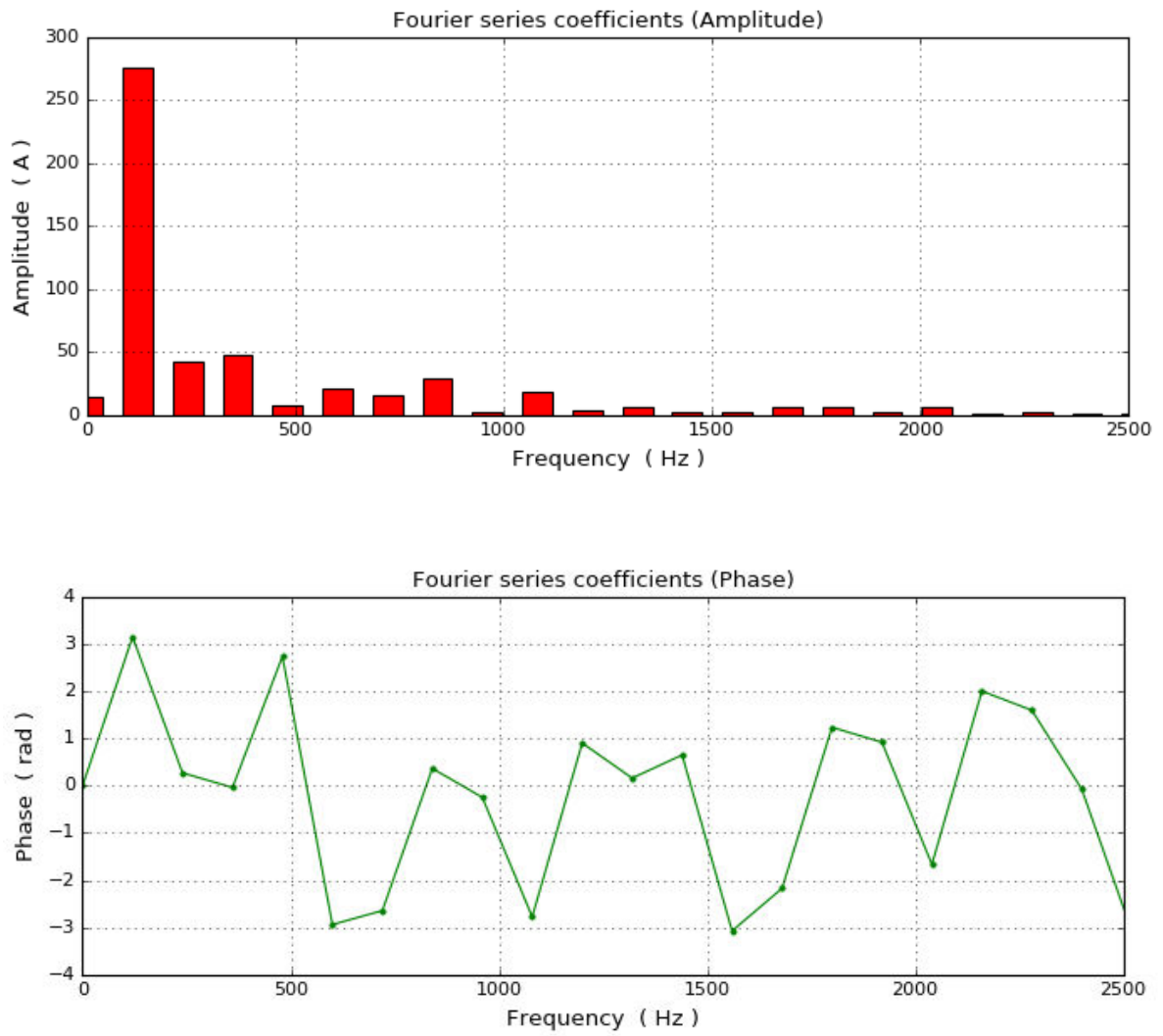


Fig. 10. Amplitude and phase of the first Fourier transform components of one of the pulses of the waveform shown in Figure 9.

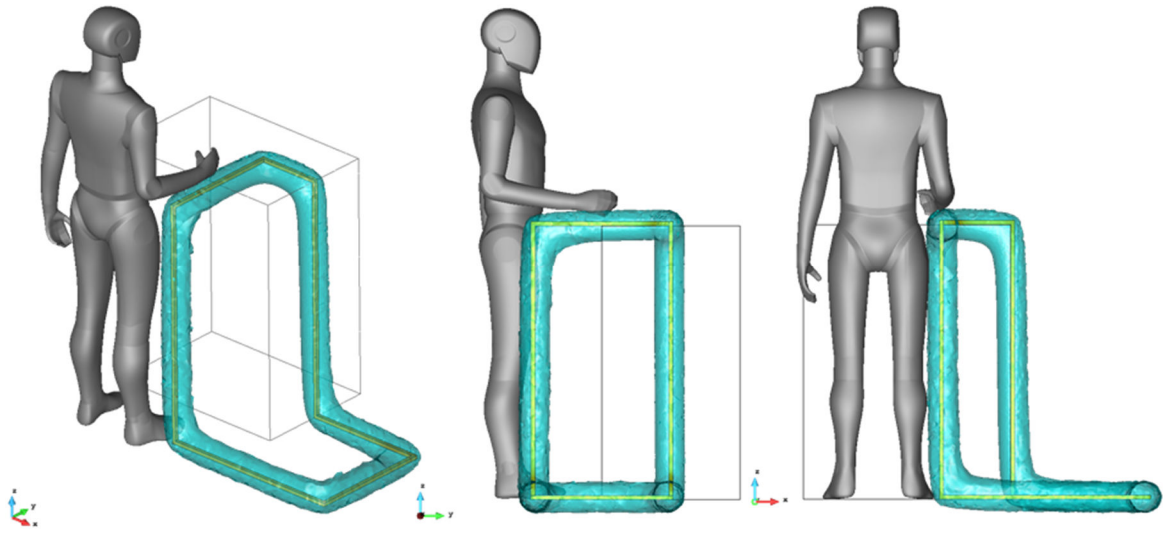


Fig. 11. TIG-AC limbs AL. Inside the light blue volume the AL is exceeded.

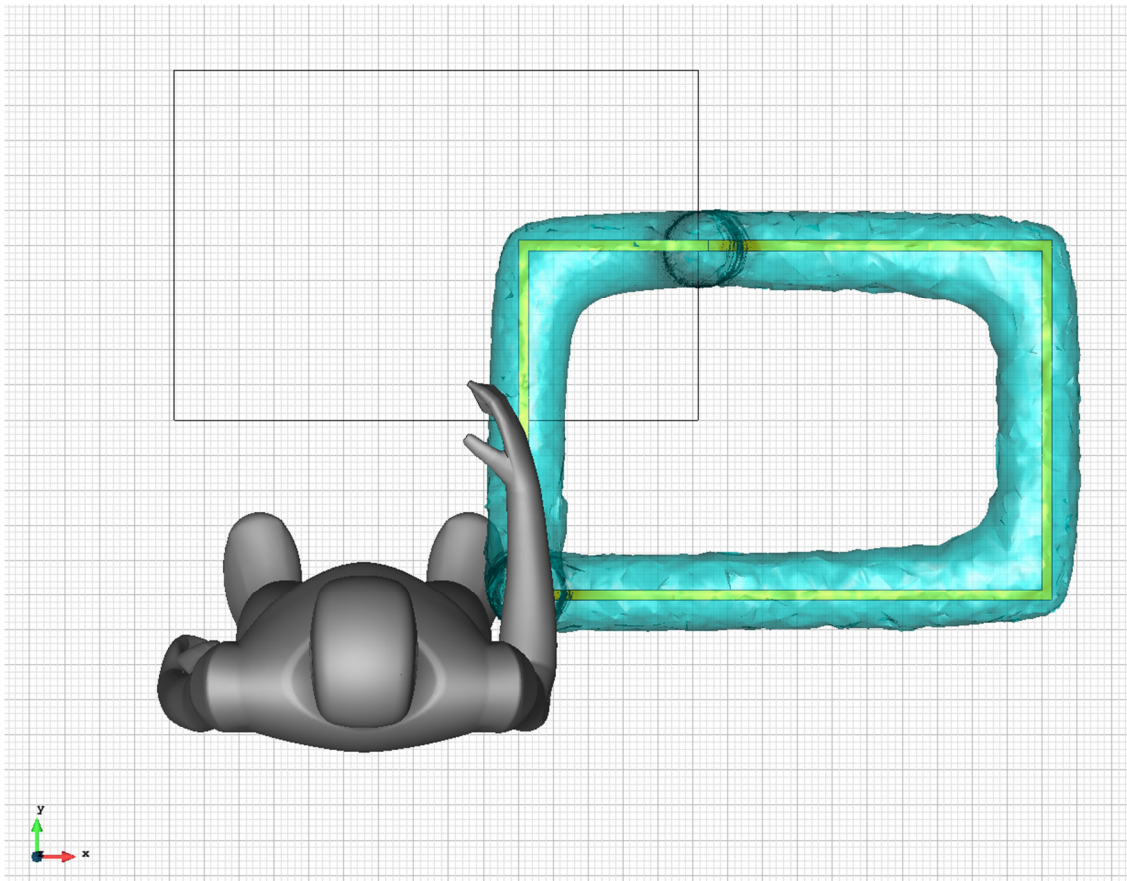


Fig. 12. TIG-AC limbs AL. The sides of each small square have a length of 1cm.

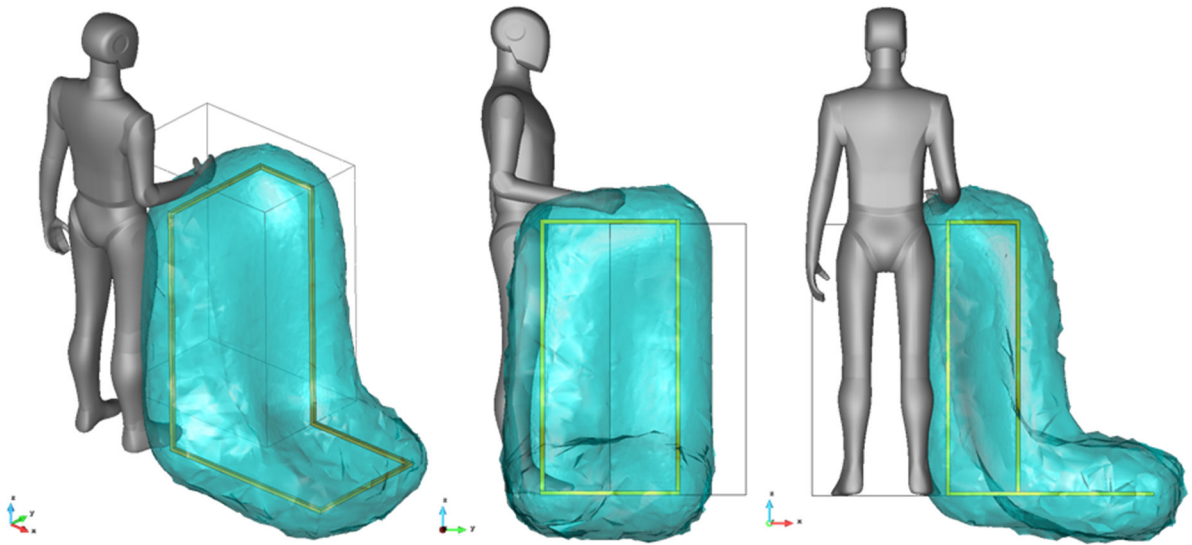


Fig. 13. TIG-AC high/low AL. Inside the light blue volume the AL is exceeded.

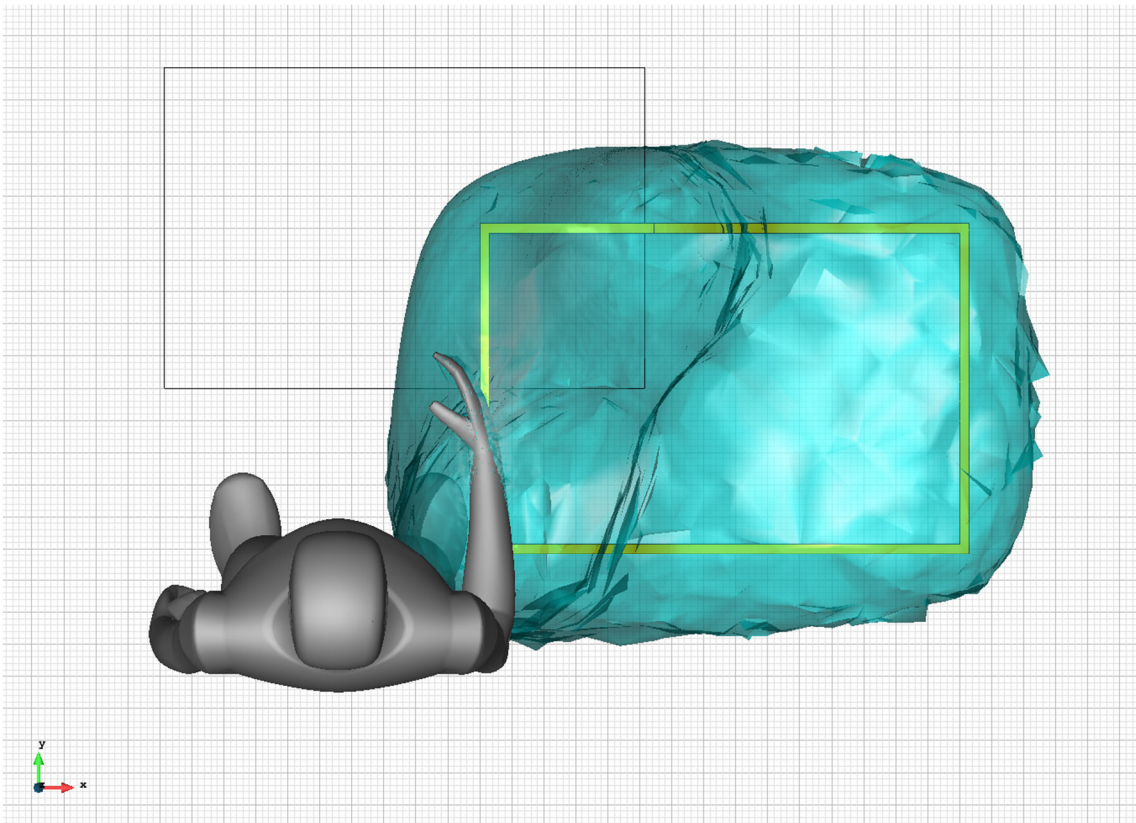


Fig. 14. TIG-AC high/low AL. The sides of each small square have a length of 1cm.

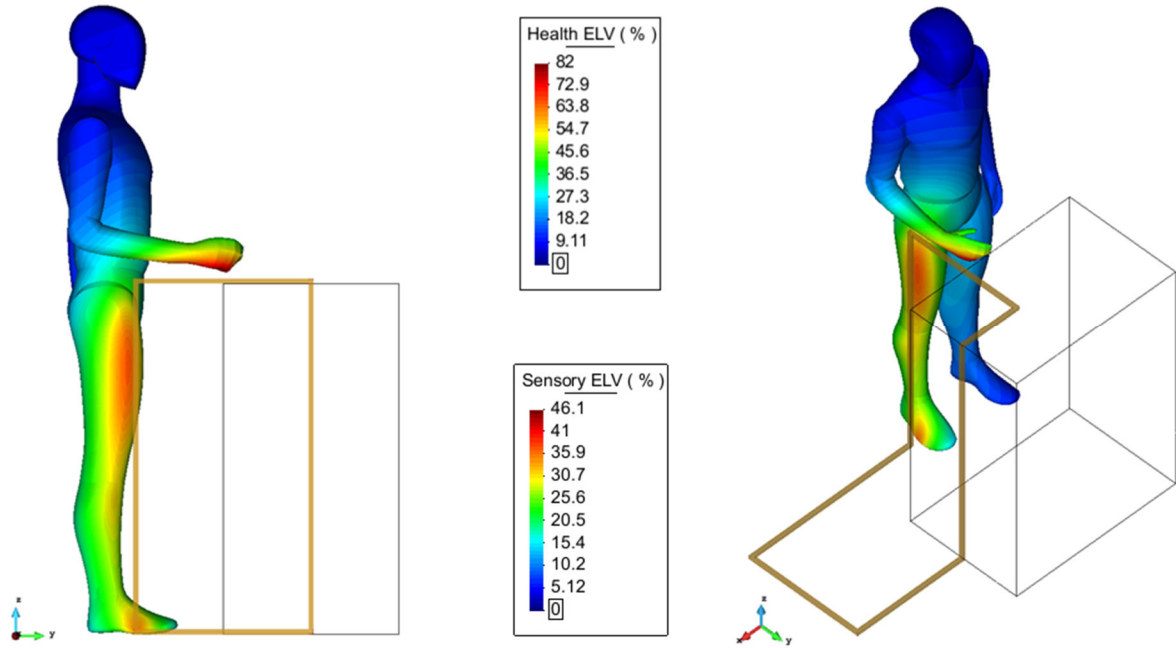


Fig. 15. TIG-AC worst-case sensory and health ELVs. Max. health ELV= 82.0% of the limit.  
 Max. sensory ELV= 46.1% of the limit. Mannequin properties:  $\epsilon_r = 1.0$ ,  $\sigma = 0$  S/m.

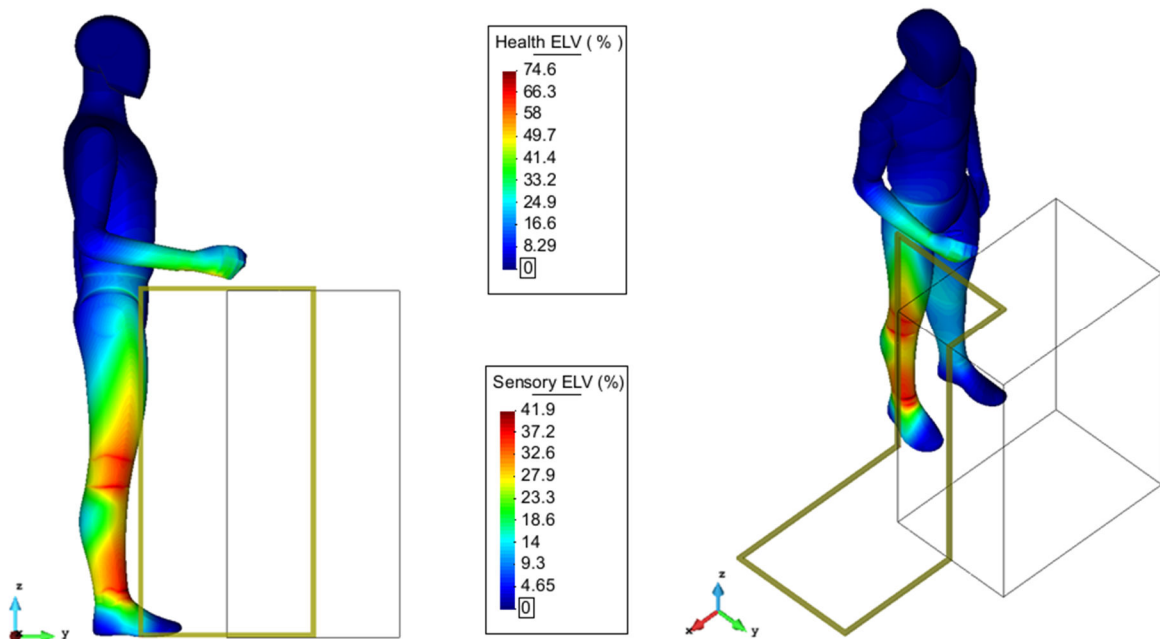


Fig. 16. TIG-AC best-case sensory and health ELVs. Max. health ELV = 74.5% of the limit.  
 Max. sensory ELV = 41.9% of the limit. Mannequin properties:  $\epsilon_r = 5e7$ ,  $\sigma = 1$  S/m.

## **4. Capacitor Discharge (CD) stud welding process**

CD welding uses large capacitors to deliver a high current pulse in a very short time. It is primarily used for welding studs to a target metallic surface preventing the need for drilling or tapping. Initially the stud has a small metal extrusion on one end called the stud pip, this is rapidly heated as the current passes through and melts resulting in an arc between the stud and the target. The hand held gun then uses a spring loaded mechanism to pressure forge the stud into the molten surface produced on the target material.

For these simulations a Taylors stud welder CD200 was used and measured using a PEM 20kA Rogowski coil set at 20kA scale with the Rogowski only wrapped once around the power cable to the torch. An example waveform from a Taylor's stud welder is shown in the next section. The peak current measured was 12.8 kA.

### **4.1. Current profiles**

Figure 17 shows the current profile analysed in this report which corresponds to a single shot Taylors CD200 stud welder on maximum heat setting. Figure 18 shows the amplitude and phase of the Fourier transform of this current pulse.

### **4.2. Action Levels**

The action levels for the CD stud welding were calculated following the steps explained in section 2.4.2. Figures 19 to 22 show the results of the simulations for the maximum setting of the Taylors CD200 stud welder (waveform in Figure 17). The ALs are exceeded so an evaluation of the ELVs is required. This evaluation is shown in the Figures 23 and 24 of the next section.

### **4.3. Exposure Limit Values**

The ELVs were calculated using the technique explained in section 2.4.3. The results are shown in Figures 23 and 24. The limits are greatly exceeded, and action must be taken to reduce the exposure of the operator.

### **4.4. Risk assessment**

The exposure limits fixed by the Directive are exceeded. Therefore, actions must be taken to reduce the exposure of the operator. Figure 22 shows that if the operator stands 125 cm away from any point on the current carrying conductor then the exposure would be below the high/low ALs and, therefore, the welding process would be compliant with the Directive. It may be possible to stand closer by calculating multiple ELVs for different operator positions. But, 125 cm is an acceptable distance and no great advantage would be gained after performing these simulations.

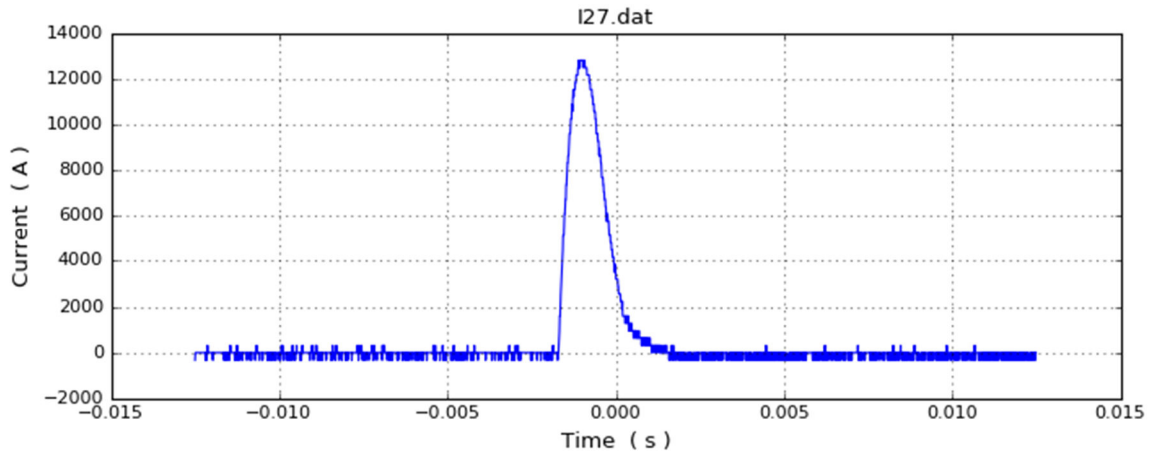


Fig. 17. Current profile of a single shot Taylors CD200 stud welder on maximum heat setting.

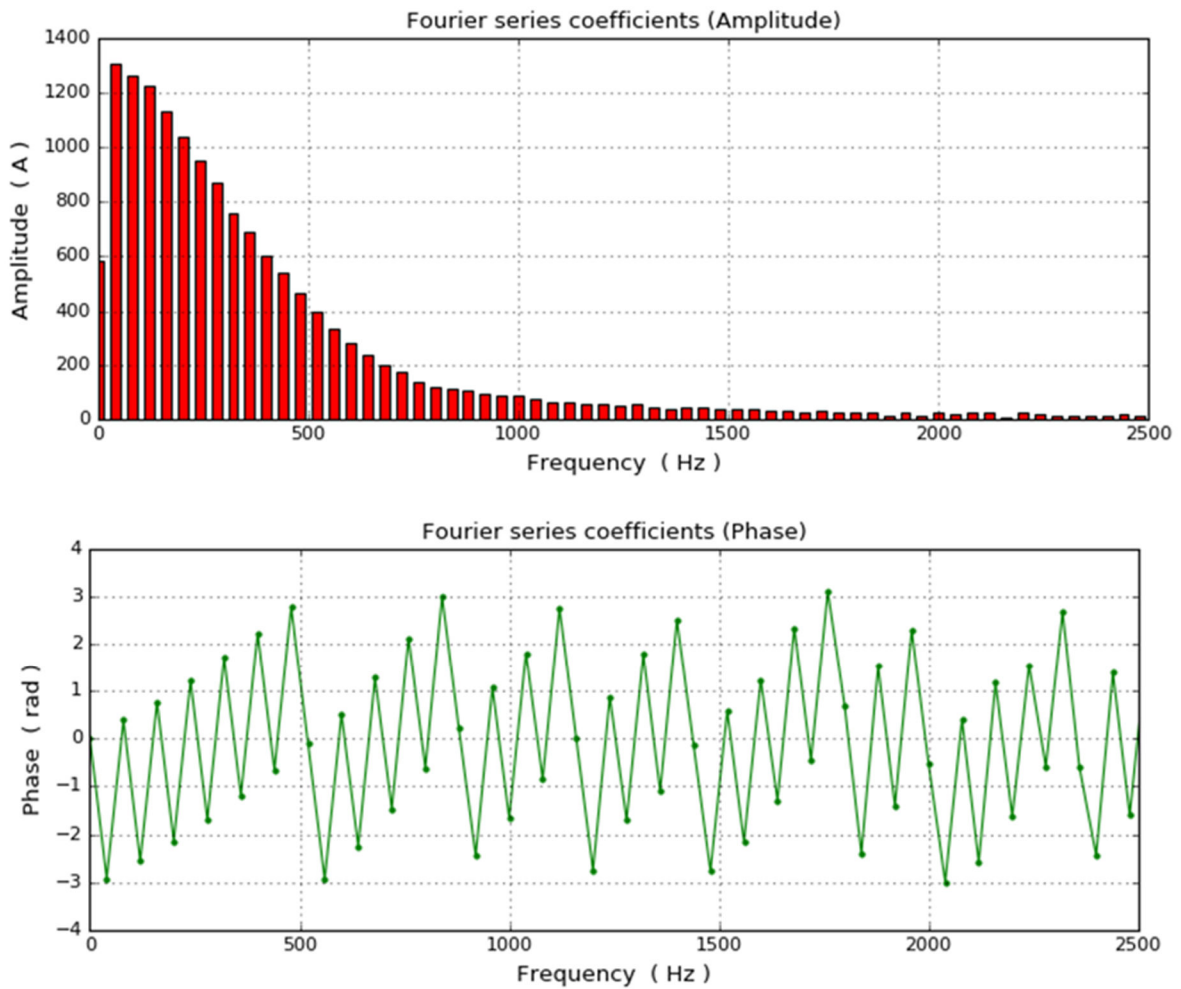


Fig. 18. Amplitude and phase of the first Fourier components of the waveform of Figure 17.

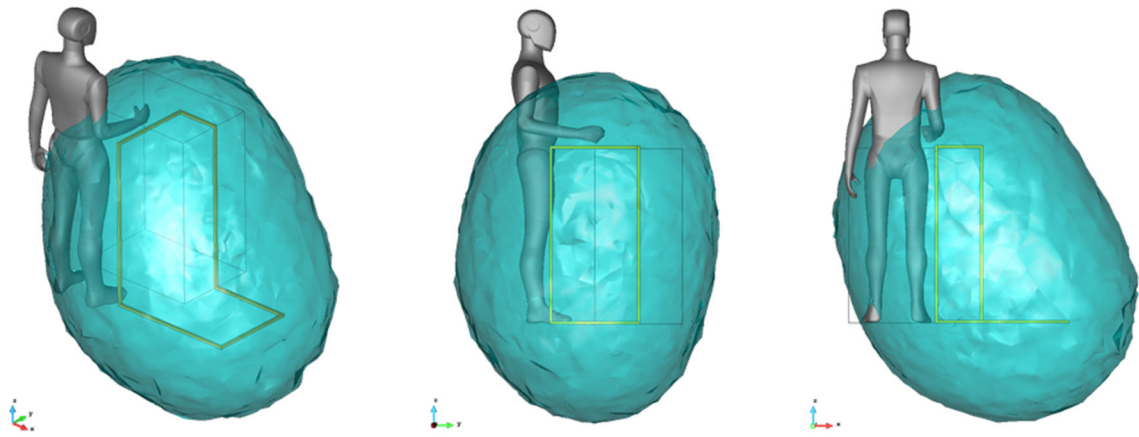


Fig. 19. CD-stud limbs AL. Inside the light blue volume the AL is exceeded.

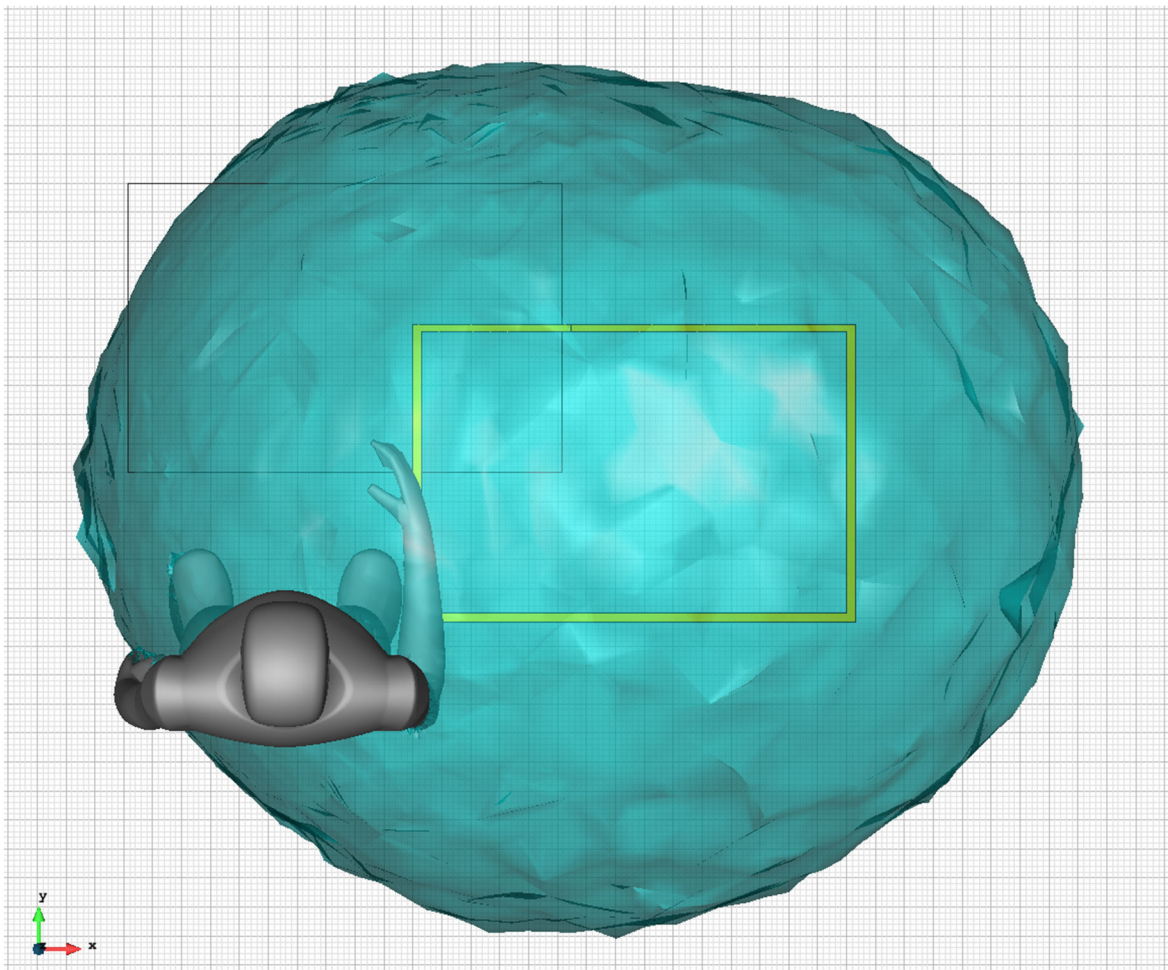


Fig. 20. CD-stud limbs AL. The sides of each small square have a length of 1cm.

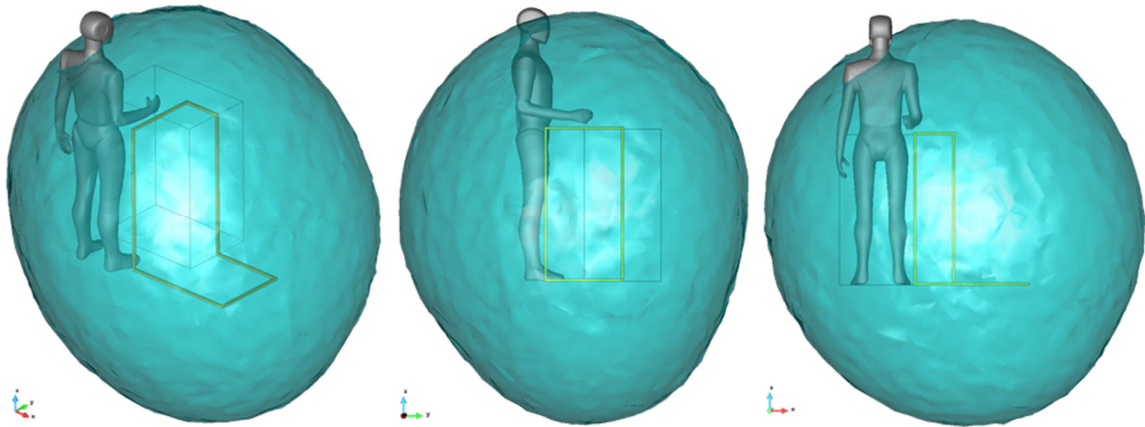


Fig. 21. CD-stud high/low **B** AL. Inside the light blue volume the AL is exceeded.

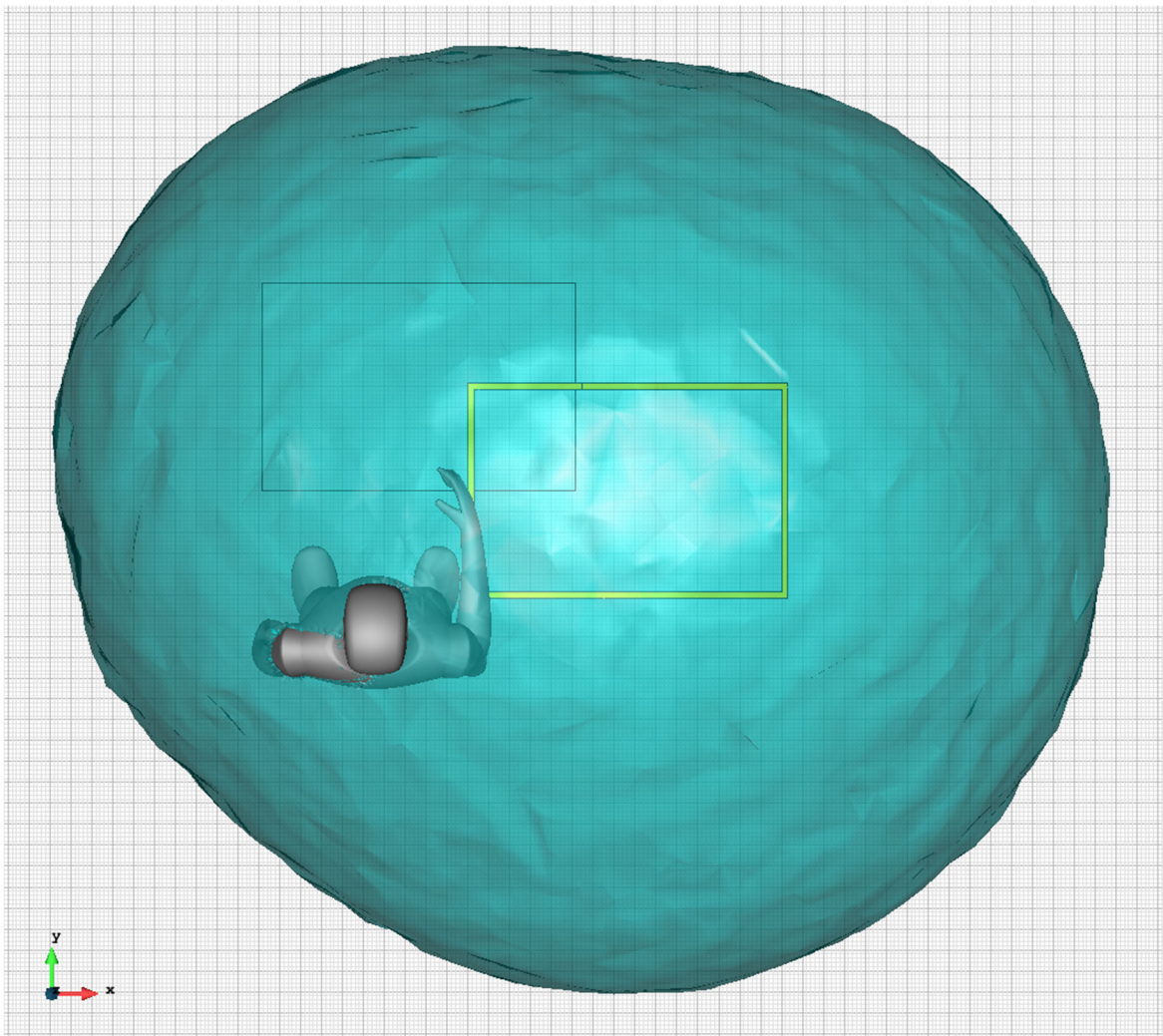


Fig. 22. CD-stud high/low **B** AL. The sides of each small square have a length of 1cm.

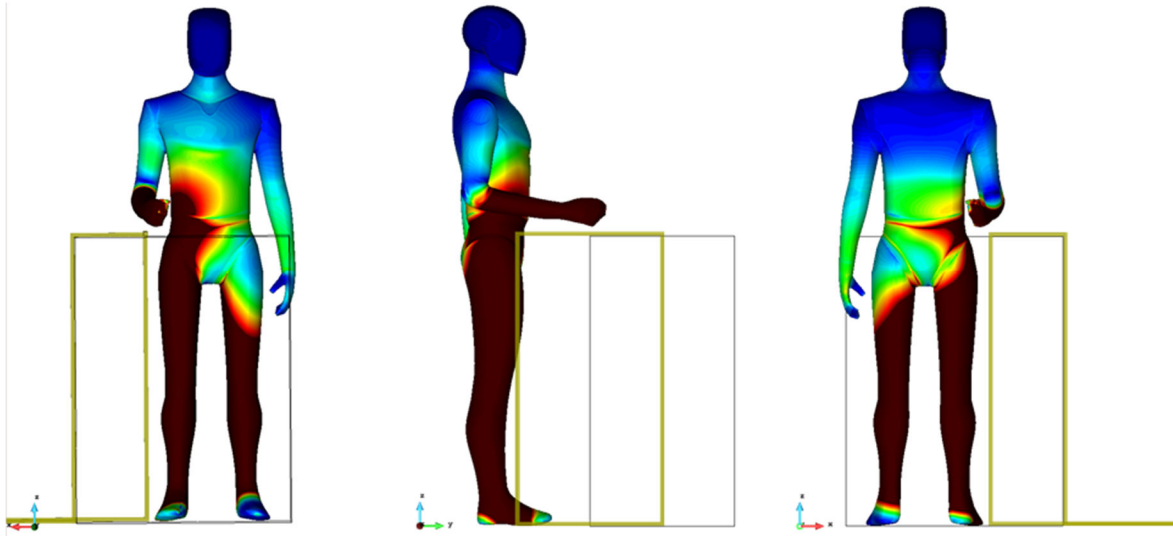


Fig. 23. CD-stud best-case sensory ELV (%). Max. sensory ELV = 700% of the limit. Dark red colour represents the area in which the levels are exceeded. Mannequin properties:  $\epsilon_r = 5e7$ ,  $\sigma = 1$  S/m.

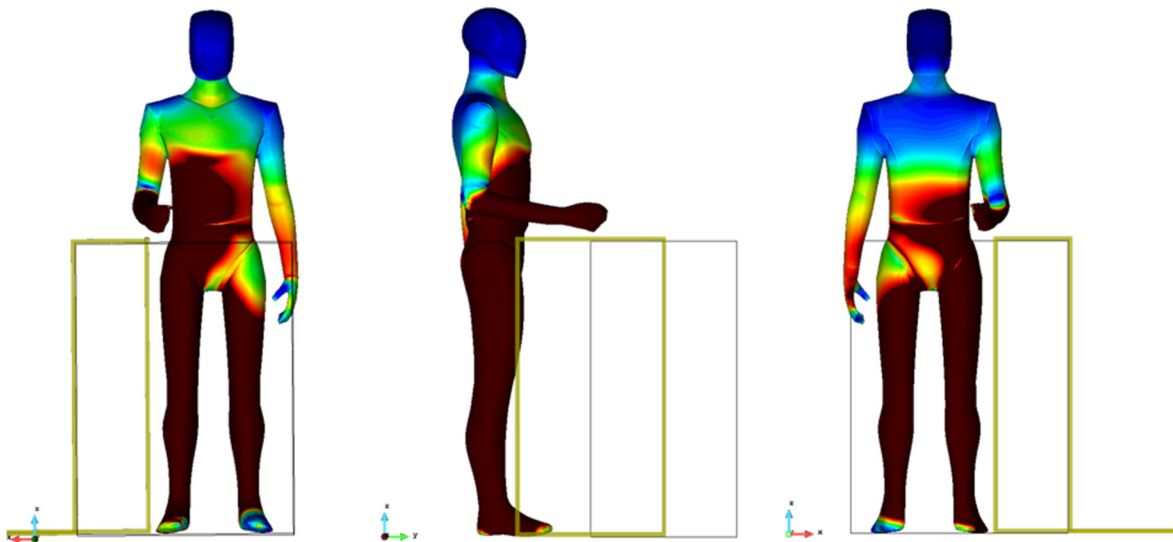


Fig. 24. CD-stud best-case health ELV (%). Max. health ELV = 1200% of the limit. Dark red colour represents the area in which the levels are exceeded. Mannequin properties:  $\epsilon_r = 5e7$ ,  $\sigma = 1$  S/m.

## **5. Summary and conclusions**

In this work two welding process were assessed against the European Union Directive 2013/35/EU. The TIG-AC process using the Kemppi MasterTIG 3500W up to its maximum setting was shown to be compliant with the Directive and no further actions are required. On the other hand, the CD-stud welding process using the Taylors CD200 on maximum setting was shown to exceed the exposure limits fixed by the EU Directive and actions must be taken to reduce the exposure of the operator. To be compliant with the Directive the operator must stand a minimum of 125 cm from any point on the current carrying cable.

## References

- [1] European Commission, "Non-binding guide to good practice for implementing Directive 2013/35/EU electromagnetic fields - Volume I: Practical Guide," Publications Office of the European Union, 2015.
- [2] R. Otin, "ERMES: A nodal-based finite element code for electromagnetic simulations in frequency domain," *Computer Physics Communications*, vol. 184 (11), pp. 2588-2595, 2013.
- [3] R. Otin, "Regularized Maxwell equations and nodal finite elements for electromagnetic field computations," *Electromagnetics*, vol. 30 (1-2), pp. 190-204, 2010.
- [4] R. Otin, "Numerical study of the thermal effects induced by a RFID antenna in vials of blood plasma," *Progress In Electromagnetics Research Letters*, vol. 22, pp. 129-138, 2011.
- [5] R. Otin, J. Verpoorte, and H. Schippers, "A finite element model for the computation of the transfer impedance of cable shields," *IEEE Transactions on Electromagnetic Compatibility*, vol. 53 (4), pp. 950-958, 2011.
- [6] R. Otin and H. Gromat, "Specific absorption rate computations with a nodal-based finite element formulation," *Progress In Electromagnetics Research*, vol. 128, pp. 399-418, 2012.
- [7] R. Otin, L. E. García-Castillo, I. Martínez-Fernández, and D. García-Doñoro, "Computational performance of a weighted regularized Maxwell equation finite element formulation," *Progress In Electromagnetics Research*, vol. 136, pp. 61-77, 2013.
- [8] R. Otin, "A numerical model for the search of the optimum frequency in electromagnetic metal forming," *International Journal of Solids and Structures*, vol. 50 (10), pp. 1605-1612, 2013.
- [9] R. Otin, R. Mendez, and O. Frutos, "A frequency domain approach for computing the Lorentz force in electromagnetic metal forming," *International Journal of Applied Electromagnetics and Mechanics*, vol. 46 (1), pp. 125-142, 2014.
- [10] R. Otin, J. Verpoorte, H. Schippers, and R. Isanta, "A finite element tool for the electromagnetic analysis of braided cable shields," *Computer Physics Communications*, vol. 191 (1), pp. 209-220, 2015.
- [11] S. Koch, H. Schneider, and T. Weiland, "A low-frequency approximation to the Maxwell equations simultaneously considering inductive and capacitive phenomena," *IEEE Transactions on Magnetics*, vol. 48 (2), 2012.
- [12] R. Hiptmair, F. Kramer, J. Ostrowski, "A robust Maxwell formulation for all frequencies," *IEEE Transactions on Magnetics*, vol. 44 (6), pp. 682-685, 2008.
- [13] P.A. Hasgall, F. Di Gennaro, C. Baumgartner, E. Neufeld, M.C. Gosselin, D. Payne, A. Klingensböck, N. Kuster, "IT'IS Database for thermal and electromagnetic parameters of biological tissues," DOI: 10.13099/VIP21000-03-0, [www.itis.ethz.ch/database](http://www.itis.ethz.ch/database), v3.0, 2015.
- [14] Electromagnetic fields in welding (EMFWELD), [www.emfweld.eu](http://www.emfweld.eu), 2016.
- [15] IEEE Standard, "Recommended Practice for Determining the Peak Spatial-Average Specific Absorption Rate (SAR) in the Human Head from Wireless Communications Devices: Measurement Techniques," 1528-2003, 2003.
- [16] IEC 62209-1, "Human Exposure to Radio Frequency Fields from Hand-Held and Body-Mounted Wireless Communication Devices—Human Models, Instrumentation, and Procedures—Part 1: Procedure to Determine the Specific Absorption Rate (SAR) for Hand-Held Devices Used in Close Proximity to the Ear (Frequency Range of 300 MHz to 3 GHz)," 2005.